Predicted Quantum Topological Hall Effect and Noncoplanar Antiferromagnetism in $K_{0.5}RhO_2$

Jian Zhou,[1] Qi-Feng Liang,[2] Hongming Weng,[3] Y. B. Chen,[4] Shu-Hua Yao,[1] Yan-Feng Chen,[1,5,*]
Jinming Dong,[4] and Guang-Yu Guo[6,7,†]

[1]*National Laboratory of Solid State Microstructures and Department of Materials Science and Engineering,*
Nanjing University, Nanjing 210093, China
[2]*Department of Physics, Shaoxing University, Shaoxing 312000, China*
[3]*Beijing National Laboratory for Condensed Matter Physics, and Institute of Physics,*
Chinese Academy of Sciences, Beijing 100190, China
[4]*National Laboratory of Solid State Microstructures and Department of Physics, Nanjing University, Nanjing 210093, China*
[5]*Collaborative Innovation Center of Advanced Microstructures, Nanjing University, Nanjing 210093, China*
[6]*Department of Physics, National Taiwan University, Taipei 10617, Taiwan*
[7]*Physics Division, National Center for Theoretical Sciences, Hsinchu 30013, Taiwan*
(Received 26 February 2016; revised manuscript received 13 May 2016; published 20 June 2016)

The quantum anomalous Hall (QAH) phase is a two-dimensional bulk ferromagnetic insulator with a nonzero Chern number in the presence of spin-orbit coupling (SOC) but in the absence of applied magnetic fields. Associated metallic chiral edge states host dissipationless current transport in electronic devices. This intriguing QAH phase has recently been observed in magnetic impurity-doped topological insulators, *albeit*, at extremely low temperatures. Based on first-principles density functional calculations, here we predict that layered rhodium oxide $K_{0.5}RhO_2$ in the noncoplanar chiral antiferromagnetic state is an unconventional three-dimensional QAH insulator with a large band gap and a Néel temperature of a few tens of Kelvins. Furthermore, this unconventional QAH phase is revealed to be the exotic quantum topological Hall effect caused by nonzero scalar spin chirality due to the topological spin structure in the system and without the need of net magnetization and SOC.

The integer quantum Hall effect (IQHE), first found in 1980 [1], is one of the most important discoveries in condensed matter physics. When a strong perpendicular magnetic field is applied to a two-dimensional (2D) electron gas at low temperatures, the Hall conductance is precisely quantized in units of the fundamental conductance quantum (e^2/h) due to Landau-level quantization. This quantization is subsequently found to be directly connected with the topological property of the 2D bulk insulating states, characterized by a topological invariant called the Chern number [2,3]. This topological understanding of the IQHE implies that the IQHE can also occur in other time-reversal symmetry (TRS) broken systems with a topological nontrivial band structure in the absence of the external magnetic field, leading to the so-called quantum anomalous Hall effect (QAHE). This effect was first proposed by Haldane in a honeycomb lattice model with a staggered magnetic field that produces zero average flux per unit cell [4]. Other model systems have also been proposed including the insulating ferromagnetic quantum wells [5], the disorder-induced Anderson insulator [6], Rashba graphene coupled with the exchange field [7,8], kagome lattice [9], and ferromagnetic Skyrmion crystal [10].

Because of its intriguing nontrivial topological properties and great potential application for designing dissipationless electronics and spintronics, extensive theoretical studies have been made to search for real materials to host such a QAHE. The conventional mechanism for the QAHE is the recognition of the QAHE as the quantized version of the anomalous Hall effect (AHE) in a ferromagnetic metal [11]. In particular, it has been recently established that the Berry curvature in the momentum space caused by the broken TRS due to the magnetization and spin-orbit coupling (SOC), acts as a fictitious magnetic field [12,13] and thus gives rise to the AHE. In a topologically nontrivial ferromagnetic insulator (Chern insulator), the integral of the Berry curvature over the Brillouin zone (BZ) results in a nonzero Chern number and hence the quantized Hall conductance [14]. Indeed, several *ferromagnetic* insulators are predicted to be the Chern insulators by first-principles band structure calculations based on this mechanism [14,15]. Importantly, based on the prediction in Ref. [15], the QAHE has recently been observed in Cr-doped $(Bi, Sb)_2Te_3$ ferromagnetic topological insulator films [16]. Nevertheless, the QAH phase appears at extremely low temperatures (less than 30 mK) due to the small band gap (less than 0.01 eV) and low carrier mobility in the sample. This hinders further exploration of the exotic properties of the Chern insulator and also its applications. Thus, it would be fruitful to search for the QAHE in crystalline magnetic insulators with a large band gap.

On the other hand, it was found in Ref. [9] that in the kagome lattice, the above-mentioned fictitious magnetic field can also be generated by the scalar spin chirality $\kappa = \sum \vec{S}_i \cdot (\vec{S}_j \times \vec{S}_k)$ (where $\vec{S}_i$, $\vec{S}_j$ and $\vec{S}_k$ denote three noncoplanar spins) due to the nontrivial spin texture in the system. Consequently, when an electron moves around a set of three noncoplanar spins, its wave function would acquire a Berry phase of $\Omega/2$ where Ω is the solid angle subtended by the three spins. This Berry phase acts as the fictitious magnetic field and generates the AHE even in an antiferromagnet (AFM). Indeed, this unconventional AHE known as the topological Hall effect (THE) was observed in noncollinear AFMs such as $Nd_2Mo_2O_7$ [17] and $Pr_2Ir_2O_7$ [18]. Nevertheless, the topological Hall conductivity detected in these materials are small, being only a small fraction of the conductance quantum (e^2/h) [17–19].

Here we predict that the easily synthesized layered oxide $K_{0.5}RhO_2$ [20,21] in the noncoplanar antiferromagnetic (nc-AFM) state (Fig. 1) would host the QAH phase with a large band gap of 0.22 eV, based on a systematic first-principles study of its magnetic and electronic properties. We also find that the QAH effect is caused by the nonzero scalar spin chirality in the noncoplanar AFM state, i.e., in the absence of the SOC and net magnetization, and thus is the quantized THE (QTHE). The calculated exchange coupling parameters between the neighboring Rh atoms reveal that the nc-AFM state is caused by the frustrated magnetic interactions in the compound, with an estimated Néel temperature of ∼20 K.

Methods.—The electronic structure of $K_{0.5}RhO_2$ has been calculated based on the density functional theory (DFT) with the generalized gradient approximation

(GGA) plus on-site Coulomb repulsion (i.e., the GGA + U scheme) (see Ref. [22] for computational details). The experimental lattice constants [30] are used. Nevertheless, the atomic positions are optimized theoretically [22]. Anomalous Hall conductivity (AHC) is calculated by using Wannier interpolation with an effective Hamiltonian constructed in a basis of maximally localized Wannier functions (MLWFs) [31]. The band structure obtained from the effective Hamiltonian agrees well with that from the DFT calculations (see Fig. S3 in Ref. [22]).

Noncoplanar antiferromagnetic structure.—K_xRhO_2 has recently received increasing attention [20,21,32–34] because it is isostructural and isoelectronic to thermoelectric material Na_xCoO_2 [35]. K_xRhO_2 crystallizes in the γ-Na_xCoO_2-type structure where the RhO_2 layer and the K layer stack alternately along the c axis [20,21], as illustrated in Fig. 1(a). Indeed, significant thermopower and the Seebeck coefficient were observed in $K_{0.49}RhO_2$ [20] and $K_{0.63}RhO_2$ [21], respectively. Furthermore, as for Na_xCoO_2, K_xRhO_2 is expected to become superconducting and also exhibit interesting magnetic behaviors at certain potassium concentration (x), which can be tuned by K de-intercalation of $KRhO_2$ [34]. In particular, Rh atoms in each RhO_2 layer form a 2D triangular lattice which was recently shown to host exotic magnetic states tunable by the band filling [36,37]. In K_xRhO_2, Rh ions would be Rh^{3+} ($4d^6$) when $x = 1$ and Rh^{4+} ($4d^5$) if $x = 0$. Thus, Rh atoms in each RhO_2 layer would have their $4d$ orbitals split into partially filled t_{2g} orbitals and empty e_g orbitals [32], and t_{2g} orbitals would be further split into occupied double e'_g orbitals and a partially occupied single a_{1g} orbital due to the trigonal deformation of RhO_2 octahedra. When $x = 0.5$, Rh ions would be $Rh^{3.5+}$ ($4d^{5.5}$) and the a_{1g} band would have a filling factor of $3/4$, which was predicted by the mean-field solution of the ferromagnetic Kondo lattice model to have a chiral magnetic ordering and spontaneous quantum Hall effect [36,37].

Here we investigate the magnetic properties of $K_{0.5}RhO_2$ with the DFT calculations. We consider all possible magnetic configurations up to four-sublattice orders on one RhO_2 monolayer (see Figs. S1 and S2 in Ref. [22]). We perform total energy calculations for these magnetic configurations within the GGA + U scheme. The calculated total energies listed in Table S1 in Ref. [22] show that the all-in–all-out noncollinear nc-AFM configuration (Fig. 1) has the lowest total energy. Importantly, the nc-AFM configuration is an insulator with a band gap of 0.22 eV, while all the other configurations are metallic.

Quantum topological Hall insulating phase.—Plotted in Fig. 2(a) is the band structure of $K_{0.5}RhO_2$ in the nc-AFM structure. Figure 2(a) shows that the system is an insulator with a band gap of 0.22 eV. To study the nature of the band gap, we further calculate the AHC. For three-dimensional (3D) quantum Hall insulators, AHC $\sigma_{AH} = n\, e^2/hc$ where c is the lattice constant along the c axis, n should be an
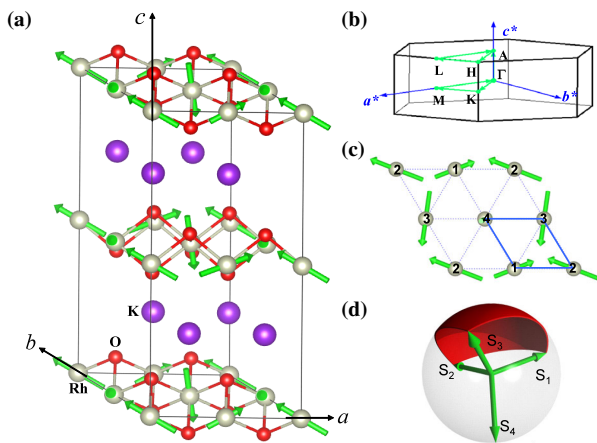

FIG. 1. (a) Crystal structure of $K_{0.5}RhO_2$ in the $2 \times 2 \times 1$ supercell and (b) its hexagonal Brillouin zone. Green arrows show the Rh magnetic moments in the noncoplanar antiferromagnetic (nc-AFM) configuration. (c) Top view of the magnetic structure in one RhO_2 layer. Thin blue lines denote the chemical unit cell. Numbers label the four Rh atoms in the planar supercell. (d) Unit sphere spanned by the four Rh magnetic moments in one RhO_2 layer parallel transported to have a common origin.
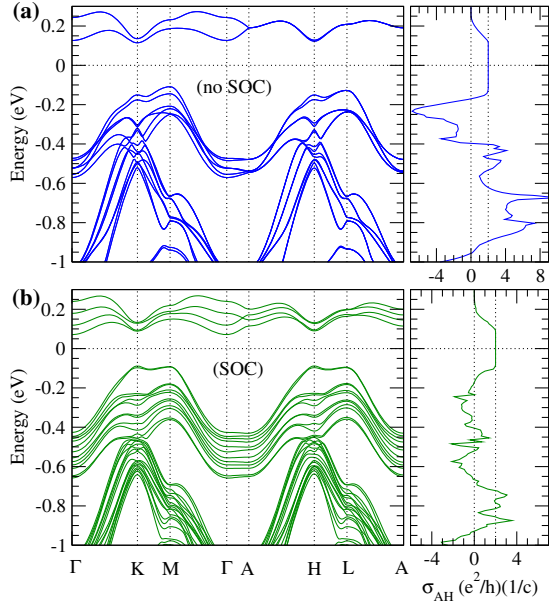
FIG. 2.   Band structure and anomalous Hall conductivity (σ_{AH}) of $K_{0.5}RhO_2$ in the noncoplanar antiferromagnetic (nc-AFM) state without SOC (a) and with SOC (b).

integer and equal to the Chern number (n_C) [38]. The calculated AHC is displayed as a function of the Fermi level in Fig. 2(a). Indeed, we find that the band gap is topologically nontrivial with the Chern number $n_C = 2.0$, and hence the system is a 3D Chern insulator. Figure 2(a) shows that the calculated AHC remains constant and is equal to 2.0 e^2/hc in the entire band gap region.

Since the total magnetization of $K_{0.5}RhO_2$ in the nc-AFM state is zero and the SOC is not included in the electronic structure calculation yet, the obtained nonzero AHC is not caused by spontaneous occurrence of magnetization and SOC [11], and hence is unconventional. Instead, the nonzero AHC results from the nonzero scalar spin chirality $\kappa = \sum \vec{S}_i \cdot (\vec{S}_j \times \vec{S}_k)$ generated by the *noncoplanar chiral* magnetism in the nc-AFM state [9,17]. In the nc-AFM state, there are magnetic moments on four Rh atoms in one RhO_2 layer (their unit vectors labelled as S_1, S_2, S_3, S_4 in Fig. 1). By parallel transporting the four unit vectors to have a common origin, we obtain a unit sphere, as shown in Fig. 1(d). Thus, the sum of the four solid angles (Ω) spanned by the four three-spin sets of $\vec{S}_1 \cdot (\vec{S}_2 \times \vec{S}_3)$, $\vec{S}_3 \cdot (\vec{S}_2 \times \vec{S}_4)$, $\vec{S}_3 \cdot (\vec{S}_4 \times \vec{S}_1)$, $\vec{S}_4 \cdot (\vec{S}_2 \times \vec{S}_1)$ is 4π. The associated Berry phase γ is then half of the total solid angle Ω and this gives rise to a Chern number of $n_C = \gamma/2\pi = 1$ [14]. Since one unit cell contains two RhO_2 layers, the Chern number of the system would be 2 and the AHC $\sigma_{AH} = 2.0$ e^2/hc. Therefore, the QAH insulating phase predicted here is entirely due to the QTHE. Finally, we note that the sign of the Chern number and AHC could be reversed by changing the all-in to all-out nc-AFM configuration (see Fig. S2 in Ref. [22]).

Chiral edge states and spin texture.—According to the bulk-boundary correspondence [39], the nc-AFM $K_{0.5}RhO_2$ would have one metallic edge state per RhO_2 layer which carries dissipationless current. To examine these interesting edge states, we calculate the energy bands for a thick $K_{0.5}RhO_2$ nanoribbon along the a axis using the MLWFs. The nanoribbon has a width of 40 unit cells along the b axis and remains periodic along the a axis and c axis. The calculated one-dimensional band structure along the a axis is shown in Fig. 3(a). We can see that there are four edge states within the bulk band gap, two localized on one edge carrying electrons along positive a direction (red lines) and two sitting on the opposite edge carrying electrons along negative a direction (blue lines), as illustrated in Fig. 3(b). We note that the direction of the dissipationless edge current can be switched by reversing, e.g., the all-in nc-AFM state to all-out one.

The spin texture of the edge state in $K_{0.5}RhO_2$ is studied by the one-band tight-binding (TB) Hubbard model analysis (see Ref. [22] for details). Figure 3(c) displays the spin texture of the A edge state near the Fermi level in a segment of the $K_{0.5}RhO_2$ ribbon. We find that the spin moments are well localized on the atoms along the edges and decay rapidly towards the interior of the ribbon.

Discussion.—In the above-mentioned electronic structure calculations, the SOC was not included. Therefore, the uncovered quantized AHC can be completely attributed to nonzero scalar spin chirality, and hence results from the genuine QTHE. Nevertheless, the SOC always exists in real materials. In particular, the SOC strength of Rh $4d$ orbitals is not small and hence cannot be ignored. To examine how
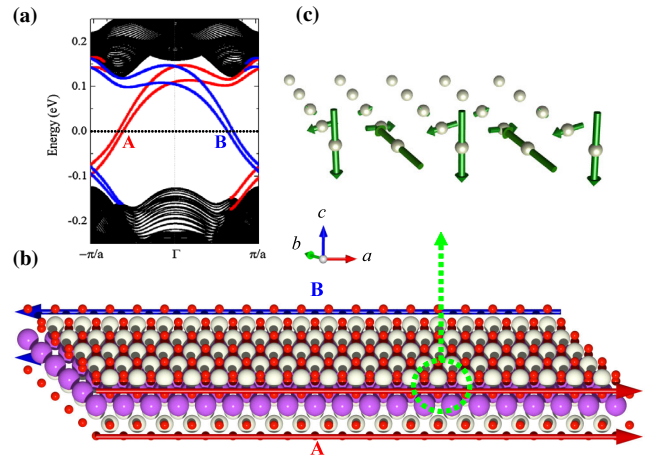

FIG. 3.   (a) Band structure of a thick noncoplanar antiferromagnetic $K_{0.5}RhO_2$ ribbon cut along the a axis. Black lines represent projected bulk energy bands, while red (A) and blue (B) lines denote chiral edge states in the bulk band gap on the two opposite sides of the ribbon. In (b), red and blue arrowed lines represent the chiral edge states A and B, respectively, one per RhO_2 layer. (c) Spin texture of the A edge state near the Fermi level in a segment of the $K_{0.5}RhO_2$ ribbon. Green vectors represent the spin moments on the Rh atoms.

the electronic structure and especially the QTHE discovered here would be affected by the SOC effect, we have repeated the calculations with the SOC included, and the calculated energy bands and AHC are shown in Fig. 2(b). It is clear from Fig. 2(b) that almost all doubly degenerate bands are now split due to the SOC. Figure 2(b) also indicates that the size of the calculated AHC below the band gap generally gets reduced when compared to Fig. 2(a), although the line shape remains similar. Importantly, Fig. 2(b) shows that the system is still an insulator with a similar band gap (0.16 eV), and also has a quantized AHC with the Chern number of 2. Interestingly, when the SOC is included, the system acquires a small magnetization of 0.08 μ_B/f.u. due to the spin canting (Table S2 in Ref. [22]). This small magnetization would provide a coupling between the magnetic structure and external magnetic field and thus allows us to control the sign of the Chern number and the direction of the edge currents by an applied magnetic field.

To understand the nc-AFM order and estimate its Néel temperature, we evaluate the exchange coupling parameters between neighboring Rh atoms in one RhO_2 layer by mapping the calculated total energies of the ferromagnetic (FM), striped (s-AFM), and zigzag (z-AFM) AFM states (see Table S1 in Ref. [22]) to the classical Heisenberg model. In so doing, we obtain the first near-neighbor exchange coupling $J_1 = 4.4$ meV (FM coupling) and second near-neighbor exchange coupling $J_2 = -3.6$ meV (AFM coupling). According to the phase diagram of the J_1-J_2 Heisenberg model [40], this implies that noncollinear magnetic states are energetically favored in $K_{0.5}RhO_2$. Furthermore, based on these parameters, a mean-field estimation (see Ref. [41] and references therein) would lead to a Néel temperature of ~20 K for $K_{0.5}RhO_2$, being well above 30 mK at which the QAHE was observed in Cr-doped $(Bi, Sb)_2Te_3$ [16]. Thus, the QTHE predicted in $K_{0.5}RhO_2$ here would provide an easily accessible platform for exploring exotic states of quantum matters and also be promising for technological applications.

To understand the formation of the topological insulating gap, we also perform a TB Hamiltonian analysis of the magnetic and electronic properties of one monolayer of $K_{0.5}RhO_2$. We consider the one-band TB Hubbard model because the two conduction bands and six top valence bands of $K_{0.5}RhO_2$ in the nc-AFM structure (Fig. 2a) are derived mainly from the Rh $4d$ a_{1g} orbital. We solve the model Hamiltonian self-consistently within the mean-field approximation (see Ref. [22] for details). We find that the nc-AFM structure (Fig. 1) is the most stable state, being consistent with the DFT calculations. Figure 4(a) shows that the TB band structure of the NM state is a metal with conduction and valence bands touching at all three M points in the BZ at the Fermi level. In the primitive unit cell, the Rh a_{1g} band is 3/4-filled and hence metallic. Therefore, in the 2×2 supercell, three of the four a_{1g} bands
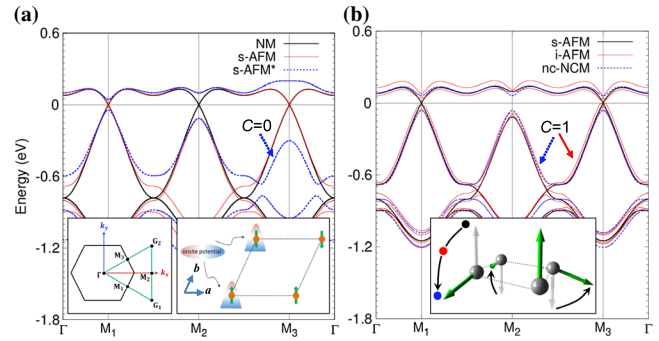

FIG. 4. (a) The TB energy bands of the NM, s-AFM, and s-AFM* states along the symmetry lines in the Brillouin zone (left inset). The s-AFM* state differs from the s-AFM state in that an onsite potential is added on one of the two sites on each ferromagnetic (FM) chain along the a axis (right inset). (b) The TB band structures of the s-AFM and nc-AFM configurations as well as an intermediate noncollinear magnetic state (i-NCM) (inset) which occurs when the s-AFM state is transformed to the nc-AFM state by spin rotations.

obtained by folding the energy bands in the primitive unit cell, are completely filled up to the BZ boundary including the M points. However, the supercell possesses three half-translation symmetries $\mathbf{a}/2$, $\mathbf{b}/2$ or $(\mathbf{a} + \mathbf{b})/2$, and consequently, the conduction and valence bands touch at the M points. Introducing the striped AFM (Fig. S1b) configuration breaks the $\mathbf{b}/2$ and $(\mathbf{a} + \mathbf{b})/2$ half-translation symmetries, and thus opens a gap at the M_2 point in the BZ. Putting an extra onsite potential on two sites in the supercell [see the right inset in Fig. 4(a)] further lifts the $\mathbf{a}/2$ half-translation symmetry and opens a gap at the M_1 and M_3 points. Therefore, the resultant AFM* state is an insulator. However, it is not a QAH insulator because the calculated Chern number $n_C = 0$.

Similarly, the nc-AFM configuration breaks the three half-translation symmetries and thus opens a gap at all three M points [Fig. 4(b)]. In contrast, the gap is nontrivial because the calculated $n_C = 1$. Note that the nc-AFM state can be obtained from the s-AFM state by rotating the four spins [see the inset in Fig. 4(b)]. Interestingly, all the intermediate states are a QAH insulating phase with $n_C = 1$, except the s-AFM state where the Chern number is ill-defined since it is a metal. This is because all the intermediate states have a nonzero scalar spin chirality with a total solid angle spanned by the four spins is 4π, as for the nc-AFM state. These results demonstrate that the QAH phase found here is robust against variation of the magnetic structure around the nc-AFM state.

As mentioned before, the nc-AFM order was recently predicted in the ferromagnetic Kondo triangular lattice (FKTL) model due to the Fermi surface nesting at the 3/4 band filling [36,37]. As found here, the nc-AFM phase is insulating and exhibits a QAHE [36,37]. Thus, the QAH phase discovered in $K_{0.5}RhO_2$ may be considered as a materialization of the predicted QAHE in the FKTL model

[36,37]. However, the magnetism in the FKTL model results from the localized electrons on the magnetic ions, while the conduction electrons in the Rh $4d$ a_{1g} orbital in $K_{0.5}RhO_2$ give rise to both the magnetism and conduction. We also notice that Hamamote *et al.* very recently predicted the QTHE in the Skyrmion crystal based on the double-exchange model [10]. In this model, the conduction electrons are assumed to strongly couple to the Skyrmion spin texture and thus acquire a Berry phase when they hop among the noncollinear spin moments. Thus, the mechanism is the same as that in the FKTL model in which the noncollinear spin moments on the magnetic ions, instead of the Skyrmions, provide the fictitious magnetic field. However, the QTHE in the Skyrmion crystal [10] differs in several significant ways from the one predicted in this Letter. For example, a strong SOC (e.g., Dzyaloshinskii-Moriya interaction or Rashba interaction) is needed to stabilize the Skyrmion crystal [10]. Furthermore, a Skyrmion crystal is formed in a ferromagnet.

J. Z. and Q. F. L. contributed equally to this work.

---

[*]yfchen@nju.edu.cn
[†]gyguo@phys.ntu.edu.tw

[1] K. V. Klitzing, G. Dorda, and M. Pepper, Phys. Rev. Lett. **45**, 494 (1980).
[2] D. J. Thouless, M. Kohmoto, M. P. Nightingale, and M. den Nijs, Phys. Rev. Lett. **49**, 405 (1982).
[3] R. B. Laughlin, Phys. Rev. Lett. **50**, 1395 (1983).
[4] F. D. M. Haldane, Phys. Rev. Lett. **61**, 2015 (1988).
[5] C. X. Liu, X.-L. Qi, X. Dai, Z. Fang, and S.-C. Zhang, Phys. Rev. Lett. **101**, 146802 (2008).
[6] M. Onoda and N. Nagaosa, Phys. Rev. Lett. **90**, 206601 (2003).
[7] Z. H. Qiao, S. A. Yang, W. X. Feng, W.-K. Tse, J. Ding, Y. G. Yao, J. Wang, and Q. Niu, Phys. Rev. B **82**, 161414(R) (2010).
[8] T.-W. Chen, Z.-R. Xiao, D.-W. Chiou, and G. Y. Guo, Phys. Rev. B **84**, 165453 (2011).
[9] K. Ohgushi, S. Murakami, and N. Nagaosa, Phys. Rev. B **62**, R6065 (2000).
[10] K. Hamamoto, M. Ezawa, and N. Nagaosa, Phys. Rev. B **92**, 115417 (2015).
[11] N. Nagaosa, J. Sinova, S. Onoda, A. H. MacDonald, and N. P. Ong, Rev. Mod. Phys. **82**, 1539 (2010).
[12] Z. Fang, N. Nagaosa, K. S. Takahashi, A. Asamitsu, R. Mathieu, T. Ogasawara, H. Yamada, M. Kawasaki, Y. Tokura, and K. Terakura, Science **302**, 92 (2003).
[13] D. Xiao, M.-C. Chang, and Q. Niu, Rev. Mod. Phys. **82**, 1959 (2010).
[14] H. M. Weng, R. Yu, X. Hu, X. Dai, and Z. Fang, Adv. Phys. **64**, 227 (2015).
[15] R. Yu, W. Zhang, H. J. Zhang, S. C. Zhang, X. Dai, and Z. Fang, Science **329**, 61 (2010).
[16] C.-Z. Chang, J. Zhang, X. Feng, J. Shen, Z. Zhang, M. Guo, K. Li, Y. Ou, P. Wei, L.-L. Wang, Z.-Q. Ji, Y. Feng, S. Ji, X. Chen, J. Jia, X. Dai, Z. Fang, S.-C. Zhang, K. He, Y. Wang, L. Lu, X.-C. Ma, and Q.-K. Xue, Science **340**, 167 (2013).
[17] Y. Taguchi, Y. Oohara, H. Yoshizawa, N. Nagaosa, and Y. Tokura, Science **291**, 2573 (2001).
[18] Y. Machida, S. Nakatsuji, S. Onoda, T. Tayama, and T. Sakakibara, Nature (London), **463**, 210 (2010).
[19] C. Sürgers, G. Fischer, P. Winkel, and H. v. Löhneysen, Nat. Commun. **5**, 3400 (2014).
[20] S. Shibasaki, Y. Nishina, I. Terasaki, K. Yubuta, and T. Kajitani, J. Phys. Condens. Matter **22**, 115603 (2010).
[21] S. H. Yao, B. B. Zhang, J. Zhou, Y. B. Chen, S. T. Zhang, Z. B. Gu, S. T. Dong, and Y. F. Chen, AIP Adv. **2**, 042140 (2012).
[22] See Supplemental Material at http://link.aps.org/supplemental/10.1103/PhysRevLett.116.256601 for Figs. S1 and S2, Tables S1 and S2, as well as computational details, which includes Refs. [23–29].
[23] B. B. Zhang, N. N. Zhang, S. T. Dong, Y. Y. Lv, Y. B. Chen, S. H. Yao, S. T. Zhang, Z. B. Gu, J. Zhou, I. Guedes, D. H. Yu, and Y. F. Chen, AIP Adv. **5**, 087111 (2015).
[24] J. P. Perdew, K. Burke, and M. Ernzerhof, Phys. Rev. Lett. **77**, 3865 (1996).
[25] P. E. Blöchl, Phys. Rev. B **50**, 17953 (1994).
[26] G. Kresse and J. Hafner, Phys. Rev. B **48**, 13115 (1993).
[27] G. Kresse and J. Furthmüller, Comput. Mater. Sci. **6**, 15 (1996).
[28] S. L. Dudarev, G. A. Botton, S. Y. Savrasov, C. J. Humphreys, and A. P. Sutton, Phys. Rev. B **57**, 1505 (1998).
[29] G.-Q. Liu, V. N. Antonov, O. Jepsen, and O. K. Andersen, Phys. Rev. Lett. **101**, 026408 (2008).
[30] K. Yubuta, S. Shibasaki, I. Terasaki, and T. Kajitani, Philos. Mag., **89**, 2813 (2009).
[31] A. A. Mostofi, J. R. Yates, Y.-S. Lee, I. Souza, D. Vanderbilt, and N. Marzari, Comput. Phys. Commun. **178**, 685 (2008).
[32] R. Okazaki, Y. Nishina, Y. Yasui, S. Shibasaki, and I. Terasaki, Phys. Rev. B **84**, 075110 (2011).
[33] Y. Saeed, N. Singh, and U. Schwingenschlogl, Adv. Funct. Mater. **22**, 2792 (2012).
[34] B. B. Zhang, S. T. Dong, Y. B. Chen, L. Y. Zhang, J. Zhou, S. H. Yao, Z. B. Gu, S. T. Zhang, and Y. F. Chen, CrystEngComm **15**, 5050 (2013).
[35] R. Schaak, T. Klimczuk, M. L. Foo, and R. J. Cava, Nature (London) **424**, 527 (2003).
[36] I. Martin and C. D. Batista, Phys. Rev. Lett. **101**, 156402 (2008).
[37] Y. Akagi and Y. Motome, J. Phys. Soc. Jpn., **79**, 083711 (2010).
[38] B. I. Halperin, Jpn. J. Appl. Phys., Suppl. **26**, 1913 (1987).
[39] A. M. Essin and V. Gurarie, Phys. Rev. B **84**, 125132 (2011).
[40] S. N. Saadatmand, B. J. Powell, and I. P. McCulloch, Phys. Rev. B **91**, 245119 (2015).
[41] J. C. Tung and G. Y. Guo, Phys. Rev. B **83**, 144403 (2011).